CrystEngComm

www.rsc.org/crystengcomm
Volume 15 | Number 39 | 21 October 2013 | Pages 7835–8050

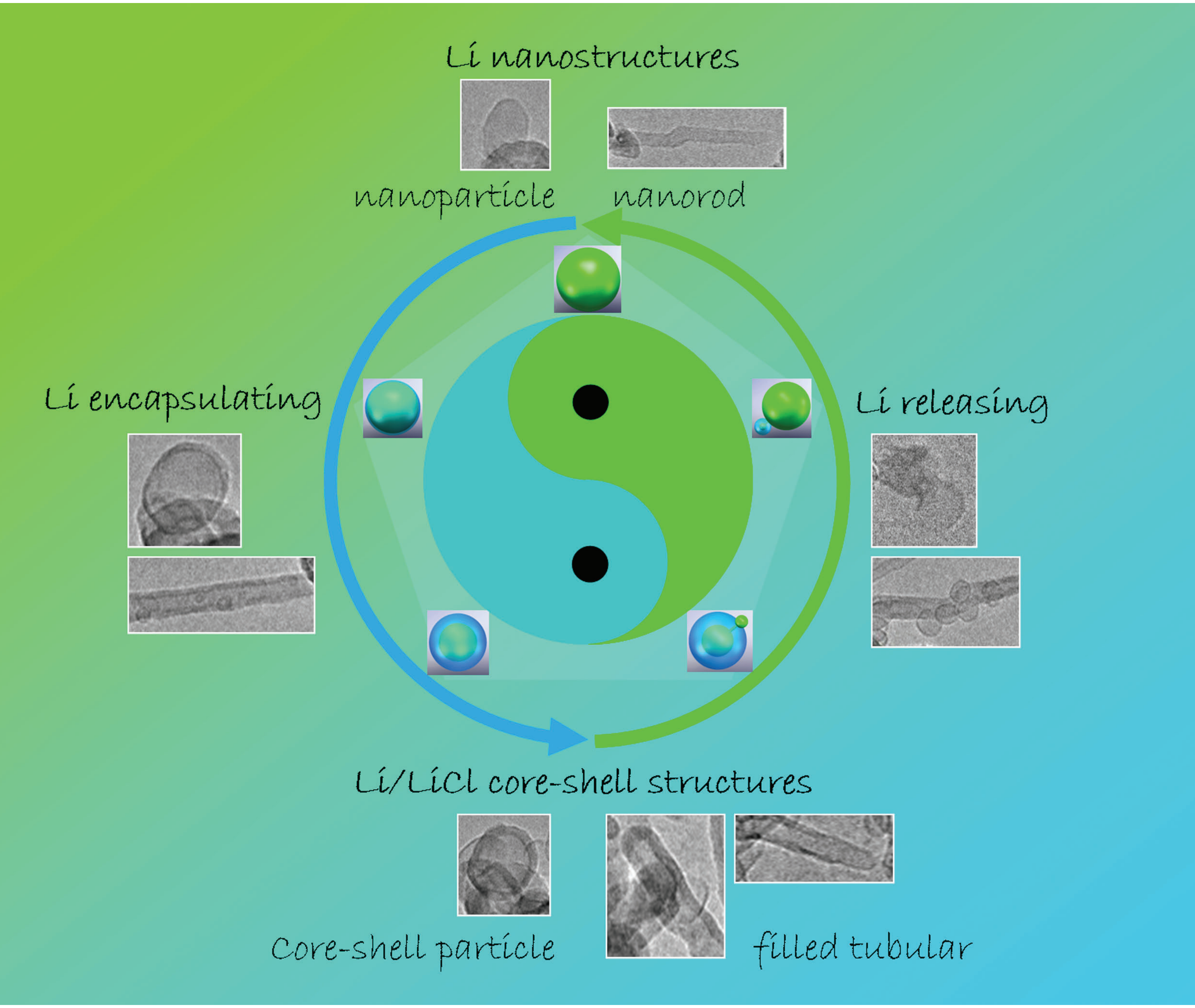

RSC Publishing

COVER ARTICLE
Neng, Li-tao *et al.*
The *in situ* TEM observation of rapid lithium encapsulation and release in LiCl nanoshells and nanotubes

CrystEngComm

RSCPublishing

PAPER

View Article Online
View Journal | View Issue

Cite this: *CrystEngComm*, 2013, **15**, 7872

The *in situ* TEM observation of rapid lithium encapsulation and release in LiCl nanoshells and nanotubes

Wan Neng,*[a] Matteo Martini,[b] Su Wei-ning,[c] Xu Ling,[c] Sun Li-tao*[a] and Shen Yu-ting[a]

Received 29th May 2013,
Accepted 10th July 2013

DOI: 10.1039/c3ce40950c

www.rsc.org/crystengcomm

In this work, we performed detailed *in situ* TEM observations of the rapid encapsulation and release of lithium in nanometric structures under e-beam irradiation. With fast kinetics, the e-beam irradiation induced the formation of a LiCl shell due to the surface reaction between lithium and the surrounding chloride. In parallel, a rapid lithium release from the LiCl surface shell underwent as a competitive process. The detailed dynamic encapsulation and releasing processes were revealed with enhanced time and spatial resolution. Lithium nanoparticles, nanorods and Li/LiCl core–shell nanoparticles and nanotubes were observed during these processes. Due to the important application of lithium materials in the energy storage field, where lithium encapsulation and releasing processes play the fundamentally important roles, our findings may trigger new application methods for lithium based energy storage, in which e-beam irradiation may be used to enhance the ultra-rapid energy harvesting or releasing process.

Introduction

Encapsulated nanostructures, typically core–shell nanostructures, can be used in many fields due to their enhanced or multifunctional properties and their special material encapsulation, transportation and releasing functions. These fields include solar cells, high efficiency catalysts, batteries, transistors and drug delivery systems. For example, many novel applications using core–shell structured quantum dots enable enhanced optical emissions.[1] Other applications include encapsulated drug delivery systems for efficient tumor targeting and multifunction medicine,[2] core–shell structures for enhanced photo-catalyst activity,[3] and core–shell structured nanowires for an enhanced energy harvesting efficiency.[4] In the formation of the core–shell structures, the encapsulation process as well as the releasing process (of the encapsulated material) are two of the most important aspects. Competing mechanisms between theses two processes are observed and affect greatly the application of the core–shell structure materials.[2] The studies and knowledge of these processes thus have a central importance in the controllable and efficient usage of the core–shell structured material.

Most of the current methods used in the preparation of the core–shell nanostructure are templated processes, where the secondary phase is formed on or inside a pre-defined precursor nanostructure. It roughly includes two kinds of method: (i) the direct deposition on the surface or inner space[5] and (ii) the surface reaction-induced material alteration (Kirkendall effect).[6] Both processes work well in the core–shell structure preparation. For the opposite process, material released from the encapsulating center may follow several different routes depending on different environmental parameters. For example, slow diffusion through the porous shell layer, which is typically seen in amorphous silica shells,[7] pressure driven rapid releasing,[8] as well as an external field enhanced releasing process.[9] In spite of the importance of the encapsulation and releasing processes on dedicated application fields, however, most of the normal experimental conditions allowed only these processes to be studied in an *ex situ* manner, where the intermediate processes were inferred indirectly from the initial (un-encapsulated/encapsulated) and final (encapsulated/released) states, and the possible intermediate dynamic processes are missed and rich information about the detailed processes remain difficult to know. For example, dynamic processes about how the encapsulation process initiates, conducts and finishes; where the releasing process initiates, expands and stops are still not clear.

---

[a] *SEU-FEI Nano-Pico Center, Key Laboratory of MEMS of Ministry of Education, School of Electrical Science and Engineering, Southeast University, 210096 Nanjing, China. E-mail: wn@seu.edu.cn; slt@seu.edu.cn*

[b] *Institut Lumière Matière – équipe FENNEC, Université Claude Bernard Lyon 1, UMR 5620 CNRS–UCBL, 69622 Villeurbanne Cedex, France*

[c] *National Laboratory of Solid State Microstructures, School of Electronic Science and Engineering and School of Physics, Jiangsu Provincial Key Laboratory of Advanced Photonic and Electronic Materials, Nanjing University, 210093 Nanjing, P. R. China*

In the current report, we used an *in situ* TEM method to study the encapsulation and releasing processes in Li/LiCl core–shell structures. Our observations found that detailed dynamic processes occurred during the rapid Li encapsulation in the LiCl shells and tubes as well as the rapid release of Li through the LiCl shell. Both processes were triggered by e-beam irradiation which allowed simultaneous fabrication and observation in a convenient and, more importantly, direct manner. Models were proposed to explain the rapid dynamics and the deep inside chemical/physical mechanisms were discussed in detail. Due to the important application of lithium materials in the energy harvesting field and the fundamental important process of the lithium encapsulation and release in energy storage batteries,[10,11] our finding may trigger new application methods for lithium based batteries, where e-beam irradiation may be used to enhance the ultra-rapid energy harvesting and release process.

Experiments

A freshly prepared diluted LiCl solution ($\sim$0.05 mol L^{-1}) was used as the source material. One droplet of the LiCl solution was dipped onto a holey carbon film that was supported on a 3 mm copper mesh. A thin liquid layer was formed on the carbon film by piping away access LiCl solution, which was then placed into a vacuum chamber and dried for several hours. White powders were seen forming on the 3 mm copper mesh after drying in the vacuum chamber. The exposure to the environmental conditions showed rapid water absorption on the sample side, which was due to the existence of strong hygroscopic LiCl. A rapid sample transfer in dry conditions and a prolonged pre-pumping section effectively reduced the water absorption in the sample. The *in situ* experiments started at least half an hour after the insertion of the sample in the high vacuum (better than 10^{-4} Pa) TEM chamber, where a cold finger was embedded (liquid nitrogen cooled externally). These cautions ensured the dry state of a water free LiCl sample.

The e-beam irradiation and observations were conducted at room temperature using a LaB_6 filament Tecnai G20 transmission electron microscope (FEI Company). The e-beam intensity was read from the measured current density at the position of the fluorescence screen, which was then compared with the CCD (Gatan 628, calibrated by Gatan) counts and normalized by magnification. The e-beam intensity used in the experiments was 60 ± 20 A cm^{-2}. A high speed CCD camera was used for the image acquisition and movie recording.

Results and discussion

Growth and encapsulation of lithium in lithium chloride nanoshells

The formation of alkaline metals by the e-beam irradiation of their fluoride or chloride salts has been demonstrated in previous papers.[12,13] The main mechanism is the electron collision induced material decomposition through radiolysis or a knock-on effect. For the electrical insulator fluoride or chloride salt, radiolysis can be realized as the main effect that cuts off the bonds by electron excitation whereas the knock-on effect induces the unbalanced loss of the alkaline metal and the halogen element. Fluoride and chloride are highly volatile while the alkaline metals trend to absorb on a sample surface, and the e-beam irradiation induces the growth of the alkaline metal nanostructures on the mother phase. For LiCl, this process is written as: $2LiCl(s) \xrightarrow{\text{e-beam}} 2Li(s) + Cl_2(g)\uparrow$, where "s" and "g" stand for solid and gas, respectively. In this process, the e-beam intensity has an evident effect on the growth velocity of the lithium nanostructures. Under a low e-beam intensity (typically $<$0.1 A cm^{-2}) the LiCl crystal was relatively stable, but under a high e-beam intensity (typically, $>$5 A cm^{-2}), evidence for the LiCl crystal decomposition could be observed.

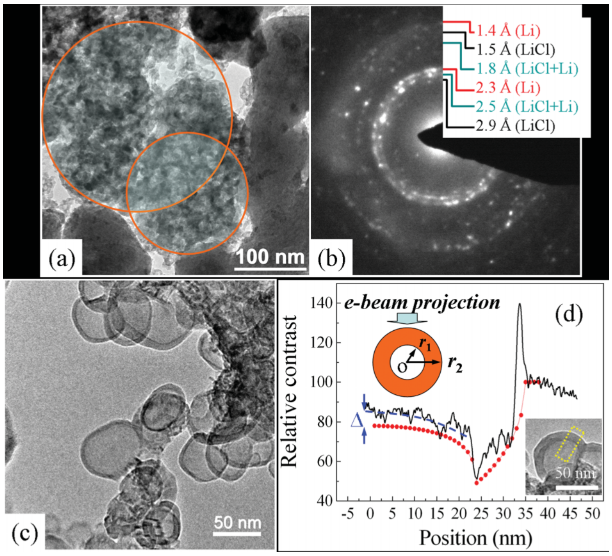

Fig. 1 (a) The TEM morphology of the LiCl samples with some zones irradiated by a focused e-beam as marked by the orange circles. (b) The SAED pattern of the irradiated LiCl, with the diffraction rings denoted. (c) The typical morphology of the lithium nanoparticles generated on the edges of the irradiated LiCl crystals. (d) The analysis of the TEM image contrast of the Li/LiCl core–shell nanostructure. The doted red line gives the calculated mass contrast for an empty shell structure, as shown in the insert carton. The black line is the line profile (dashed yellow) of a core–shell structure as shown in the insert TEM image. Note that the sharp rise (in the line profile) at the surface of the nanoparticle comes from defocus, but not the mass contrast.

Fig. 1(a) shows the TEM morphology of the LiCl sample with some regions having been irradiated by a focused e-beam as indicated by the orange circles. The image highlights a morphological difference between the irradiated and un-irradiated regions. The porous structures seen in the irradiated region indicate material decomposition, while the un-irradiated region remains dark and condensed. A careful analysis of the select area electron diffraction (SAED) pattern of the irradiated region found the coexistence of the lithium (JCPDF #: 780840) and LiCl (JCPDF #: 040664) phase (Fig. 1(b)). Moreover, the lithium nanostructures were found growing

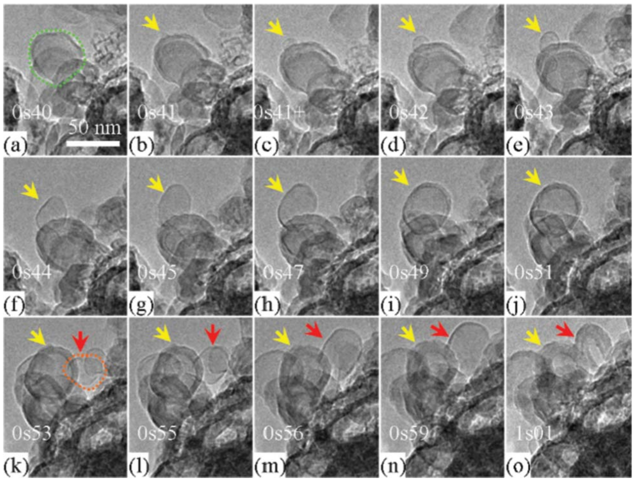

Fig. 2 (a–o) Sequential TEM images of the growth process of the lithium encapsulation in LiCl. The growth process was initiated in (b) as indicated by a yellow arrow. The dashed green circle in (a) indicates a pre-existing particle. The dashed orange circle in (k) indicates another new grown particle with the similar growth process. The images have the same magnification.

around the edges of the irradiated LiCl crystals (Fig. 1(b) and (c)). A typical morphology of the lithium nanoparticles (with a LiCl shell structure) is shown in Fig. 1(c). To study the core–shell profile of the nanoparticles (Fig. 1(d)), the contrast of the TEM image (black line) was compared with the calculated mass-thickness contrast (red dotted line) using an empty shell structure. The alignment of the experimental and calculated curves illustrated a contrast discrepancy ($\varDelta$) in the core region due to the presence of a Li/LiCl core–shell structure (since only the Li and LiCl phases were found from SAED studies). This structure is also verified by the observation of a very rapid growth process and a morphology cycling under the continuous e-beam irradiation[13] as is discussed in the following sections.

Detailed information about the rapid growth process is captured by the high speed CCD camera and reported in the series of images (Fig. 2(a)–(o)). As indicated by a yellow arrow in Fig. 2(b), a small nuclei formed on a pre-existing nanoparticle (outlined by dashed green circle in Fig. 2(a)), which expanded rapidly in the first 0.10 s (Fig. 2(b)–(h)) until a surface shell started to grow. The detailed dependence of the core (Li) and the core + shell (Li + LiCl) diameter of the core–shell structure with growth time is shown in Fig. 3. The first stage growth of the lithium nanoparticle showed a very rapid growth velocity of 310 nm s^{-1}, which was averaged in the first 0.10 s. Deceleration is noticed at the end of this region, followed by a second stage slow growth (velocity ∼38 nm s^{-1}) of the core–shell structure, according to our previous report.[12] The main reason for this is probably due to the reduced lithium absorption onto the particle surface by the formation of a LiCl encapsulation layer. The growth of the surface LiCl also caused the evident reduction of the core lithium diameter, giving a ∼17 nm diameter reduction within 0.16 s. In both cases the reaction of $2Li(s) + Cl_2(g) \rightarrow 2LiCl(s)$ is the main mechanism, which works for the encapsulation and the consumption of the lithium core from both an outward and inward direction, respectively. These processes are schematically shown in Fig. 3. Consider the consumption of the lithium core. As the lithium has the molar mass of 6.94 g mol^{-1} and density of 0.53 g cm^{-3}, while the LiCl has the molar mass of 42.394 g mol^{-1} and density of 2.068 g cm^{-3}, a simple calculation gives that the Li–LiCl transformation causes a volume reduction according to $V_{LiCl}/V_{Li} = 0.783$, which gives a change of diameter: $R_{LiCl}/R_{Li} = 0.922$. It seems that the consumption of the core region lithium finally produces voids which leads to an empty LiCl shell, as shown in the model given in Fig. 3(b). Although the formation of a sphere-shaped empty LiCl shell was not observed, we found in our intensive TEM observations that most of the nanostructures collapsed soon after the formation of a rough and porous thin LiCl shell. This can be partly caused by the generation of voids inside the LiCl shell.

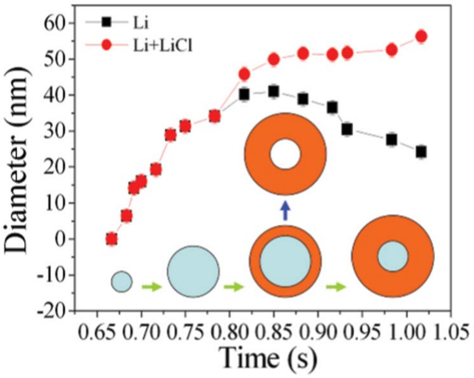

Fig. 3 The time dependence of the inner (Li) and outer (Li + LiCl) diameters of the core–shell structures. The insert shows the growth model of the lithium phase in the LiCl encapsulation process.

Referring to similar a phenomenon observed in the e-beam irradiation of NaCl and LiF,[12,13] this process is concluded to be the first stage in the lithium growth and the second stage in the LiCl formation on the surface, caused by the reaction of the lithium particle and the de-composited chloride species. This mechanism induced the rapid encapsulation of the lithium particle inside the LiCl shell. The rapid surface reaction, due to the chemically active lithium and chloride, caused a rapid surface encapsulation process. The inter-diffusion of the lithium and chloride may work as the driving force. It is also inferred that the chloride concentration should not be quite large around the lithium nanostructures, or the latter may be transferred totally into the LiCl with a continuous chemical reaction and efficient inter-diffusion. This can be due to the relatively small e-beam irradiation area compared with a large vacuum chamber that enables the efficient dispersion of the decomposited chloride species. It also can be a reason that enables the observation of a pure lithium phase and the transient surface encapsulation processes.

Rapid lithium release from the LiCl nanoshells

As mentioned above, the structure finally collapsed because the surface LiCl was not condense-packaged and more

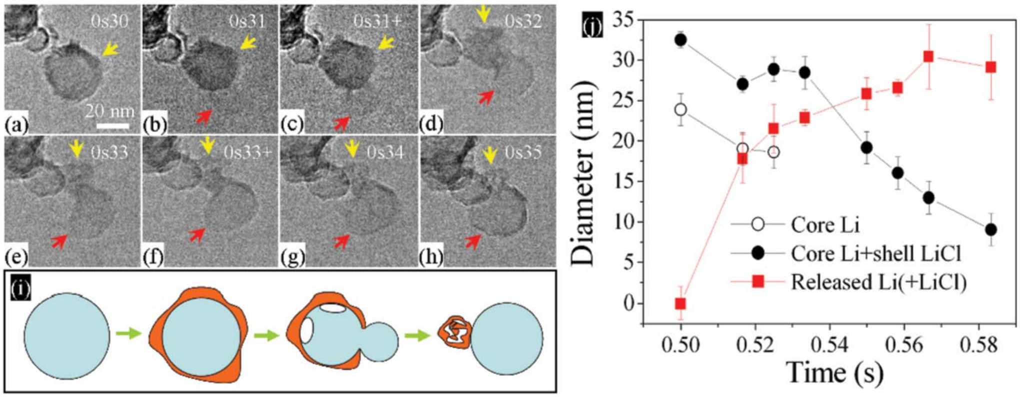

Fig. 4 (a–h) Sequential TEM images showing the rapid release of the lithium encapsulated in the Li/LiCl structure. Scale bar = 20 nm. (i) A model showing the lithium release process. (j) The time dependence of the diameters of the core Li, the Li + LiCl and the released Li (possibly with some surface LiCl, especially for the last two data points). The data for the ''core Li'' after 0.53 s are not captured because of the weak contrast of the edges in the TEM images.

importantly it was not e-beam irradiation resistant. The collapse of the Li/LiCl encapsulated structures accompanied the rapid release of the core lithium. A typical process is shown in Fig. 4(a)–(h). In Fig. 4(a), the initial Li/LiCl core–shell structure with an outer diameter of 32.5 nm and an inner Li diameter of 23.9 nm is shown, which was then found to shrink with the accompanied lithium release from the sidewall (Fig. 4(b)–(e)). The initial LiCl shell was collapsed gradually to a 9.0 nm sized agglomerate in Fig. 4(h)). The time dependence of the diameters of the core Li, the Li + LiCl and the released Li (+LiCl) (Fig. 4(j)) show a clear relationship between the initial Li/LiCl structures and the released Li, that is, the former decreases with the increase of the latter. The whole process finished within 0.10 s, giving a rapid release process, or equally, also a rapid (new) lithium nanoparticle growth rate (release/growth rate: ~500 nm s^{-1}) that accords to the above observations. Also noted is a rapid diameter increase in the released Li comparing with a moderate diameter decrease in the mother Li + LiCl structure around 0.52 s, which indicates that voids may be created inside the LiCl shell. These voids could accelerate the succeeding LiCl shell collapse.

The rapid lithium release process is schematically shown in Fig. 4(i). The lithium nanoparticles were assumed to have a smooth surface. Later, they were encapsulated in a porous and rough LiCl shell. The rough surface could result from the e-beam irradiation of the initial smooth LiCl surface or it may not have been intrinsically smooth due to its react-growth formation process, which generated some weak points or interface channels between the LiCl grains for the lithium release. The e-beam irradiation of the LiCl shell could trigger and enhance the lithium release. Moreover, the fast diffusion of Li out from the core also generates voids and further promotes the collapse of the LiCl shell, which finally generates another lithium nanoparticle absorpted on the LiCl shell agglomerate. According to our *in situ* observations, the encapsulation–release process occurs on the new lithium nanoparticle and cycles many times, where the collapsed nanoparticle itself can work as a new seed for the encapsulation–release processes.

The lithium nanorod growth and fast encapsulation

Beside the formation of the core–shell lithium nanostructures, the TEM images reveal that the e-beam irradiation could also accentuate the growth of Li nanorods. Although the different conditions for growing particles or nanorods are still unknown, we normally found the simultaneous growth of these two types of growth modes, which grew in the same time and same area, indicating that they could growth under quite similar conditions. A typical Li nanorod growth process is shown in Fig. 5(a)–(l). A nanorod with an almost constant diameter of ~15 nm was observed growing rapidly along its longitude direction. From the dependence of the length on the time as shown in Fig. 5(m), a two sectional growth dynamic was found, including a first section of rapid Li nanorod growth and a secondary sectional nanorod degradation/length shortening. For the rapid Li nanorod growth section, a growth rate of ~2.6 μm s^{-1} was found, which is much larger than that found in the Li nanoparticles. Indeed, after comparing with some currently known reports,[14,15] we found that this growth velocity is the most rapid. Also, as indicated in the figures by blue arrows, kinks were found along the Li nanorod, but they showed little effect on the large growth rate. The secondary sectional growth shows length diminishing accompanied with surface LiCl formation, which is induced by the same mechanism as discussed in the LiCl encapsulation of the lithium particles. Surface roughing was clearly seen and part of the nanorod was seen to collapse. Comparing with the evident change of the growth rate along the length direction, growth along the radical direction was much slower. The diameter growth in the first section was almost neglectable, which also showed just a limited increase due to the formation of the surface LiCl in the secondary section.

The surface reaction with chloride produces a structure where lithium was encapsulated inside the LiCl nanotube. These kinds of structure were intensively observed as shown in Fig. 6(a)–(c) and (f). In Fig. 6(a), a close-end LiCl nanotube was seen (see also the model in Fig. 6(d)). It shows uniform wall thickness and a closed tip as indicated by a red arrow. This closed tip tubular structure could be caused by a reaction with

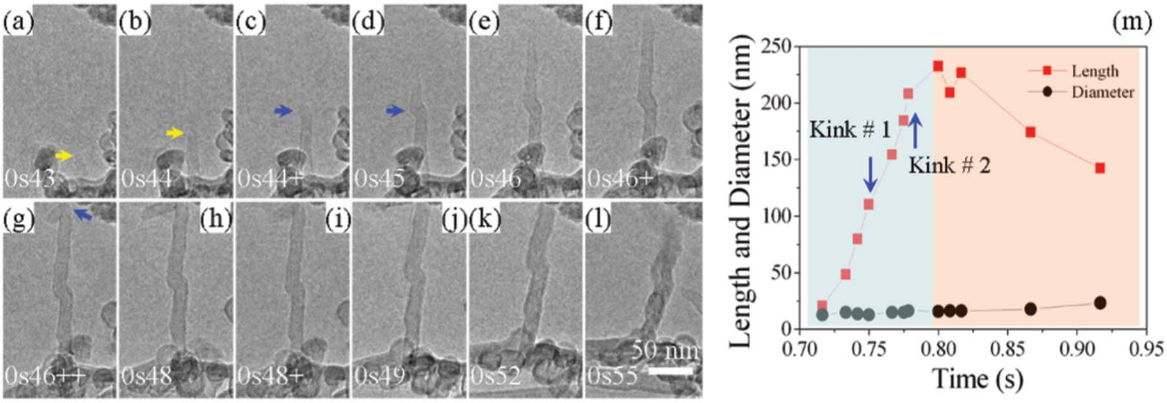

Fig. 5 (a–l) Sequential TEM image showing the growth of a lithium nanorod structure. The yellow arrows shown in the first two images indicate the tip of the lithium nanorods. The blue arrows indicate the kinks. (m) The dependence of the length and diameter on the growth time. The two sectional growth processes are marked by two colored bands.

the surrounding chloride at the end of the lithium nanorod growth period. Fig. 6(b) shows an open-end LiCl nanotube (see also the model in Fig. 6(d)). It shows diminishing wall thickness along its growth direction with an open-end tip as indicated by a red arrow. This structure could be formed due to the incomplete LiCl wall formation on the initial lithium nanorod considering the fact that the lithium–chloride reaction could take place during the lithium nanorod growth. Under this mechanism, the open-ended Li/LiCl tube structure will finally transfer into a close-ended tube structure by a continuous surface reaction. Although this phenomenon was not observed due to the fact that the Li/LiCl tube structures grow and collapse rapidly, it is believed that the lithium nanorod growth and the simultaneous surface LiCl layer formation plays the most important roles in the lithium encapsulation by LiCl tubes. Further verification of the tubular structure can be seen in the TEM image shown in Fig. 6(c) and a TEM contrast analysis shown in Fig. 6(e). The former shows a tube with its longitude direction aligned with the e-beam projection direction as indicated by a red arrow, the tubular structure can be seen clearly in this figure; the latter shows a comparison of the contrast line profile across a tube structure with a calculated contrast line profile across an empty tube structure, the discrepancy at the core region again indicates a encapsulated Li/LiCl structure.

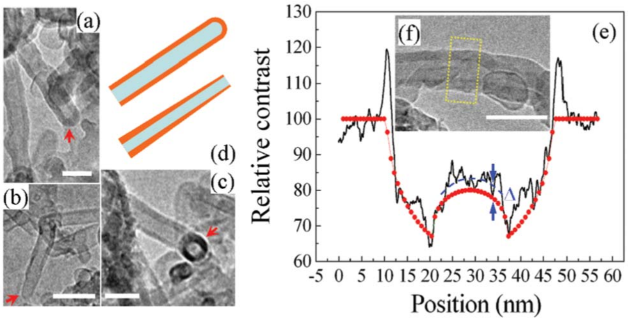

Fig. 6 TEM images showing (a) the close-end lithium-encapsulated LiCl tubular structure, (b) the open-end lithium-encapsulated LiCl tubular structure, and (c) a tube with its longitude direction aligned with the e-beam projection direction. The red arrows indicate the position of the tubular structures. (d) Structure models of the close-end (upper part) and open-end (lower part) lithium-encapsulated LiCl tubular structures. (e) A comparison of the contrast line profile across a tube structure (see insert TEM image, (f)) with a calculated contrast line profile across an empty tube structure. (f) A TEM image showing a tube structure, where a dotted yellow region was used to analyze the contrast line profile shown in (e). Scale bars = 50 nm.

The rapid lithium release from the LiCl nanotubes

The releasing of lithium from the encapsulated LiCl nanotubes also showed very rapid dynamics. It is seen that the whole lithium releasing process can be finished in the time scale of 0.25 s (see Fig. 7(a)–(k)). As shown in Fig. 7(a), the initial nanorod structure (as seen between two dashed yellow lines, which were drawn following the shape of the nanorod) showed a smooth surface with no evident LiCl layer. Later, small sized lithium particles were seen formed on the nanorod as indicated by red arrows in Fig. 7(b). The smallest lithium particle observed has a diameter ∼3 nm, which expands quickly in a short time (see Fig. 7(b)–(f)) until a size comparable with the nanorod diameter is reached. The merging of adjacent lithium particles was observed as indicated by the yellow arrows in Fig. 7(c) and (d). Accompanied with the particle growth, a LiCl layer covers gradually the initial lithium nanorod, which can be seen clearly in Fig. 7(f) and (g), but the surface LiCl layer did not stop the lithium particle growth, implying the effect of Li diffusion though the LiCl layer. Subsequently (Fig. 7(f)–(h)), the nanorod diameter decreases from 21 nm to 13 nm whereas the lithium particles continued to grow. We thus infer that the lithium particles were released from the LiCl tube, following a similar mechanism that has been discussed above. The lithium release induced the shrinking of the LiCl tube diameter. This mechanism finally resulted in the bending and collapsing of the whole structure, as shown in Fig. 7(i)–(k), with lithium particles on its surface. Fig. 7(l) (mimics the shape in Fig. 7(i)) shows a structure model of the curved lithium nanorod structure with a surface LiCl covering and

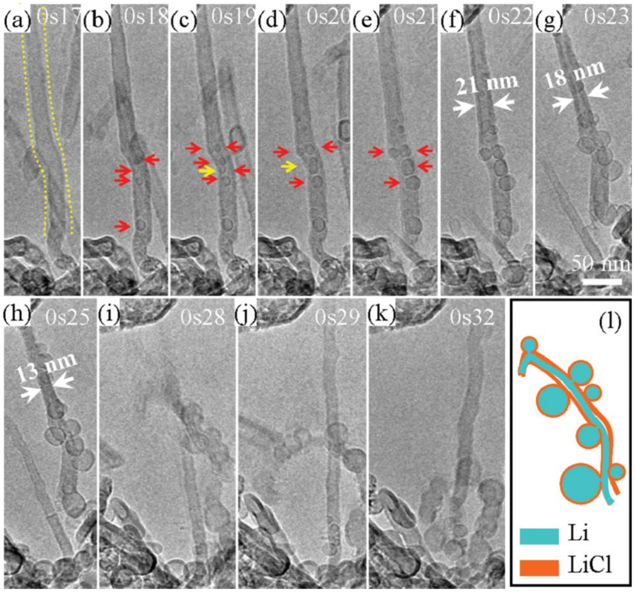

Fig. 7 (a–d) Sequential TEM images showing the rapid lithium releasing from the Li/LiCl tubular structure. The dotted yellow lines in (a) highlight the lithium nanorod studied. The red arrows indicate the release of the lithium particles. The yellow arrows show the merging of adjacent lithium particles. (l) A structure model of the curved lithium nanorod structure with a surface LiCl covering and lithium particles released on its surface, which mimics the shape in (i). All images share the same scale bar.

lithium particles released on its surface. Lithium could be release from weak points or interface channels between the LiCl grains. This process results in void generation inside the LiCl nanotube, which promoted the bending and finally the collapse of the nanotube skeleton structure.

The mechanisms of the rapid lithium encapsulation and release

The whole processes observed during our *in situ* TEM experiments are concluded in Fig. 8. The growth of the lithium nanostructures, the surface encapsulation by the LiCl shell or nanotube and the lithium release are the three key processes. During these processes, the high reactivity between the lithium and chloride and the e-beam induced decomposition of the LiCl plays the main and also competition mechanisms. As the lithium nanostructures were located in a locally chloride rich atmosphere in the small e-beam irradiated region, they will trend to react and form a surface LiCl layer, even during their short and rapid growth period. In this period the lithium nanostructure growth and surface reactions compete with each other. At the end of which the formation of a LiCl layer slows down the growth velocity of the lithium nanostructures and finally forms a LiCl shell structure.

The formation of LiCl on the lithium also competes with its decomposition that is induced by e-beam irradiation. The latter process has two effects: 1) it destroys the LiCl structure and produces a small amount of lithium residue. As the amount of lithium generated by the surface LiCl decomposition is much smaller compared with that of the released lithium observed in the experiments, and also the experiment

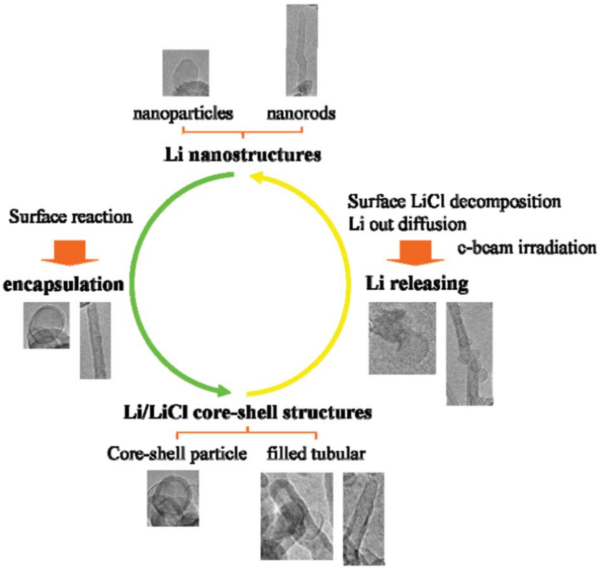

Fig. 8 The whole process of the lithium encapsulation and release during the *in situ* TEM observations as depicted schematically.

fact shows that large part of the surface LiCl is indeed kept until the structure failure, it is believed that the lithium release is not a direct process due to surface LiCl decomposition. Instead, it is realized that 2) the surface LiCl decomposition induces the formation of structure imperfections in the surface LiCl layer, such as weak points or interface channels between the LiCl grains as discussed above, which provide channels for the lithium release from the LiCl encapsulation (see Fig. 4(i) and 7(l)). In this period the formation of a LiCl layer on the lithium nanostructure surface and the e-beam irradiation induced LiCl decomposition are two competitive factors. Indeed, in most cases the LiCl layer cannot growth to a large thickness, indicating that the e-beam irradiation balanced and finally cancelled the LiCl layer growth. It is also noted that due to the large inter-diffusion coefficient especially for lithium, the limited LiCl layer thickness could not be caused by the limited diffusion length of Cl^- or Li^+.[16] It is concluded that the e-beam irradiation of the LiCl layer triggered and promoted the rapid lithium release process.

Summary

In this work, we performed detailed *in situ* TEM observations of the rapid lithium encapsulation and release under e-beam irradiation. We found that both processes can be finished within a short period in nanostructures smaller than 50 nm. During these processes, lithium nanoparticles, nanorods and Li/LiCl core–shell structured nanoparticle and nanotube were observed. The dynamic observation of the lithium encapsulation and release processes unveiled the involved mechanism including an e-beam induced lithium growth, a surface LiCl formation due to the reaction between the surface lithium and the surrounding chloride, and an e-beam irradiation of the surface LiCl layer induced (encapsulated) lithium release. A model based on the competition of these mechanisms was proposed to explain the encapsulation and release processes. Due to the important application of lithium materials in the energy harvesting field, we suggest possible recycling of lithium using an e-beam irradiation method.

Acknowledgements

This work is supported by the National Basic Research Program of China (Grant Nos. 2011CB707601 and 2009CB623702), the National Natural Science Foundation of China (Grant Nos. 51071044, 60976003 and 61006011), the Specialized Research Fund for the Doctoral Program of Higher Education (Grant Nos. 20100092120021 and 20100092110014) the Program for New Century Excellent Talents in University (NCEF-09-0293) and the Open Research Fund of State Key Laboratory of Bioelectronics.

References

1 F. Zhang, R. C. Che, X. M. Li, C. Yao, J. P. Yang, D. K. Shen, P. Hu, W. Li and D. Y. Zhao, Direct imaging the upconversion nanocrystal core–shell structure at the subnanometer level: shell thickness dependence in upconverting optical properties, *Nano Lett.*, 2012, **12**, 2852.

2 N.-H. Cho, T.-C. Cheong, J. H. Min, J. H. Wu, S. J. Lee, D. Kim, J.-S. Yang, S. Kim, Y. K. Kim and S.-Y. Seong, A multifunctional core–shell nanoparticle for dendritic cell-based cancer immunotherapy, *Nat. Nanotechnol.*, 2011, **6**, 675.

3 C. S. Pan, J. Xu, Y. J. Wang, D. Li and Y. F. Zhu, Dramatic activity of $C_3N_4/BiPO_4$ photocatalyst with core–shell structure formed by self-assembly, *Adv. Funct. Mater.*, 2012, **22**, 1518.

4 S.-H. Tsai, H.-C. Chang, H.-H. Wang, S.-Y. Chen, C.-A. Lin, S.-A. Chen, Y.-L. Chueh and J.-H. He, Significant efficiency enhancement of hybrid solar cells using core–shell nanowire geometry for energy harvesting, *ACS Nano*, 2011, **5**, 9501.

5 S. B. Yoon, B. C. Woo, S. J. Chung and W. S. Yun, Fabrication of nanoporous TiO_2 hollow capsules using core–shell silica nanoparticle templates, *J. Nanosci. Nanotechnol.*, 2012, **12**, 1604.

6 A. Zak, L. Sallacan-Echer, A. Margolin, M. Genut and R. Tenne, Insight into the growth mechanism of WS_2 nanotubes in the scale-up fluidized-bed reactor, *Nano*, 2009, **4**, 91.

7 K.-I. Sano, T. Minamisawa and K. Shiba, Autonomous silica encapsulation and sustained release of anticancer protein, *Langmuir*, 2010, **26**, 2231.

8 F. Q. Song, M. Han, M. D. Liu, B. Chen, J. G. Wan and G. H. Wang, Experimental observation of nanojets formed by heating PbO-coated Pb clusters, *Phys. Rev. Lett.*, 2005, **94**, 093401.

9 A. Schloßbauer, A. M. Sauer, V. Cauda, A. Schmidt, H. Engelke, U. Rothbauer, K. Zolghadr, H. Leonhardt, C. Bruchle and T. Bein, Cascaded photoinduced drug delivery to cells from multifunctional core–shell mesoporous silica, *Adv. Healthcare Mater.*, 2012, **1**, 316.

10 M. Gu, I. Belharouak, A. Genc, Z. Wang, D. Wang, K. Amine, F. Gao, G. Zhou, S. Thevuthasan, D. R. Baer, J.-G. Zhang, N. D. Browning, J. Liu and C. Wang, Conflicting roles of nickel in controlling cathode performance in lithium ion batteries, *Nano Lett.*, 2012, **12**, 5186.

11 M. Gu, Y. Li, X. Li, S. Hu, X. Zhang, W. Xu, S. Thevuthasan, D. R. Baer, J.-G. Zhang, J. Liu and C. Wang, In situ TEM study of lithiation behavior of silicon nanoparticles attached to and embedded in a carbon matrix, *ACS Nano*, 2012, **6**, 8439.

12 N. Wan, L.-T. Sun, X.-H. Hu, Y.-Y. Zhu, Z. Lin, X. Tao, H.-C. Bi, J. Sun and F.-Z. Dong, Charge supported growth and superplasticity of sodium nanostructures, *Cryst. Growth Des.*, 2012, **12**(8), 3899–3905.

13 J. Ghatak, W. Guan and G. Möbus, In situ TEM observation of lithium nanoparticle growth and morphological cycling, *Nanoscale*, 2012, **4**, 1754.

14 S. S. Oh, D. H. Kim, M.-W. Moon, A. Vaziri, M. Kim, E. Yoon, K. H. Oh and J. W. Hutchinson, Indium nanowires synthesized at an ultrafast rate, *Adv. Mater.*, 2008, **20**, 1093.

15 E. Auer, A. Lugstein, S. Löffler, Y. J. Hyun, W. Brezna, E. Bertagnolli and P. Pongratz, Ultrafast VLS growth of epitaxial β-Ga_2O_3 nanowires, *Nanotechnology*, 2009, **20**, 434017.

16 D. Ruzmetov, V. P. Oleshko, P. M. Haney, H. J. Lezec, K. Karki, K. H. Baloch, A. K. Agrawal, A. V. Davydov, S. Krylyuk, Y. Liu, J. Y. Huang, M. Tanase, J. Cumings and A. A. Talin, Electrolyte stability determines scaling limits for solid-state 3D Li ion batteries, *Nano Lett.*, 2012, **12**, 505.